ACS Energy LETTERS

http://pubs.acs.org/journal/aelccp

Lateral $PtSe_2$ p–n Homojunction Formation via Selective Surface Doping for Self-Powered Temperature Sensing

Seonhye Youn, Jeongmin Kim,* Sangkil Lee, Minseung Gyeon, Joonho Bang, Taehoo Chang, Hongjae Moon, Dong Hwan Kim, Kibum Kang,* and Wooyoung Lee*

Cite This: *ACS Energy Lett.* 2025, 10, 6466–6473

Read Online

ACCESS | Metrics & More | Article Recommendations | Supporting Information

ABSTRACT: Two-dimensional material-based p–n junctions are widely used in nano- and microelectronic devices. Compared to conventional doping methods, surface-charge-transfer doping provides a reliable, simple, and nondestructive approach to modulating carrier properties of 2D materials. However, despite its advantages, this method has not been used to form p–n junctions for thermoelectric applications. This paper introduces a lateral p–n homojunction temperature sensor, fabricated via simple on-sheet chemical doping of a transition metal dichalcogenide (TMDC) nanosheet grown by chemical vapor deposition. While five-layer $PtSe_2$ is semimetallic, area-selective surface doping with benzyl viologen and Magic Blue is used to suppress ambipolar transport and define distinct n-type and p-type regions. The resulting Seebeck coefficient difference between the two regions enables sensitive detection of temperature gradients, with a resolution of ∼0.1 K. This doping-based approach avoids complex processing and structural damage, offering both high sensitivity and fabrication simplicity. Our method offers a scalable route for fabricating p–n homojunctions in 2D materials, and can thus be employed to develop self-powered, high-resolution temperature sensors for a broad range of applications, from chip-scale devices to biomedical applications.

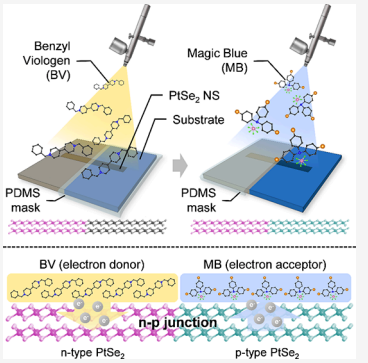

Temperature sensing is crucial in diverse domains, including industrial process control, laboratory environments, and medical applications. Various temperature sensors, including thermocouples, thermistors, and resistance temperature detectors (RTDs), have been developed for such applications. Thermocouples are widely used owing to their robust durability and stable performance over a broad temperature range. A thermocouple typically consists of either (i) a metal–metal heterojunction or (ii) a junction between p-type and n-type thermoelectric materials. Temperature is determined by the Seebeck voltage from the difference in Seebeck coefficients of the two materials. In this study, we created a p–n homojunction thermocouple using a single $PtSe_2$ nanosheet by locally tuning its Seebeck coefficient via surface doping. Ultrathin thermoelectric devices based on two-dimensional (2D) nanomaterials such as transition metal dichalcogenides (TMDCs), graphene, and black phosphorus have been extensively investigated to date. These 2D materials offer excellent tunability of electronic and thermal transport properties via thickness-dependent band engineering, and are thus promising candidates for next-generation thermoelectric platforms. Representative examples include MoS_2 nanosheets, which can achieve a thermoelectric figure of merit ($ZT = S^2\sigma T/\kappa$) exceeding 1, where S, σ, T, and κ denote the Seebeck coefficient, electrical conductivity, absolute temperature, and thermal conductivity, respectively.[1] Enhanced thermoelectric power factors ($S^2\sigma$) have also been reported in bilayer WSe_2 and black phosphorus through gate-induced carrier modulation.[2,3] Notably, $PtSe_2$ nanosheets, with tunable transport characteristic across semimetallic and semiconducting regimes realized via layer control, have emerged as versatile platforms for nanoscale thermoelectric device design.[4] Beyond thickness control, doping is critical for tailoring electronic and thermoelectric properties of 2D materials. However, conventional doping techniques for fabricating nanoscale p–n junctions, such as ion implantation, plasma treatment, and lithography-based patterning, require complex processes and may cause structural damage or increase processing costs. In contrast, surface-charge-transfer doping (SCTD) offers a facile, postsynthesis route to precisely control doping concentrations

Received: August 3, 2025
Revised: October 31, 2025
Accepted: November 21, 2025

https://doi.org/10.1021/acsenergylett.5c02461
ACS Energy Lett. 2025, 10, 6466–6473

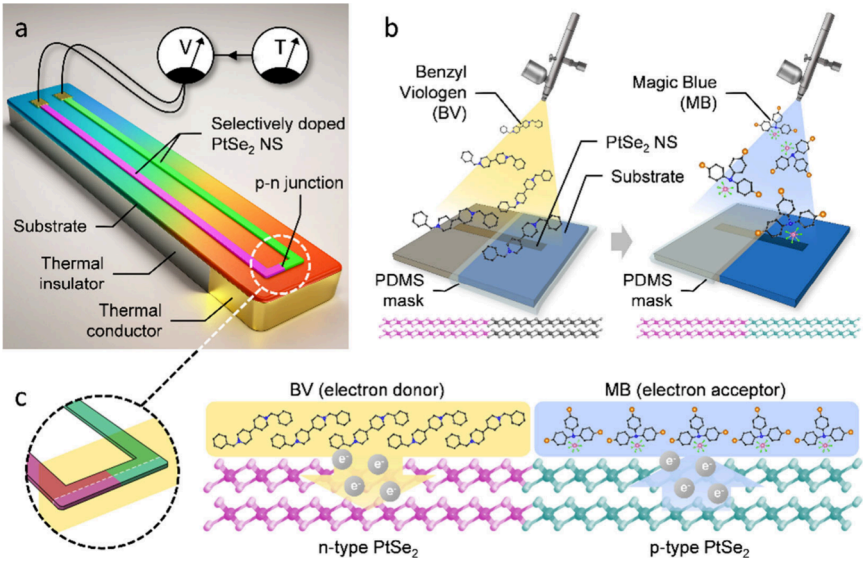

Figure 1. (a) Schematic of the self-powered temperature sensor based on a surface-doped $PtSe_2$ p−n homojunction thermocouple. The temperature difference formed across the $PtSe_2$ nanosheet on the substrate can be monitored by measuring the thermoelectric voltage between electrodes on both sides of the p−n junction. (b) Concept of area-selective SCTD using BV as an n-type dopant and MB as a p-type dopant. The doping was performed via airbrush spray coating with a PDMS mask to define the lateral p−n homojunction. (c) Mechanism of SCTD. BV molecules donate electrons to the $PtSe_2$ nanosheet, inducing n-type doping, while MB molecules withdraw electrons from the nanosheet, inducing p-type doping.

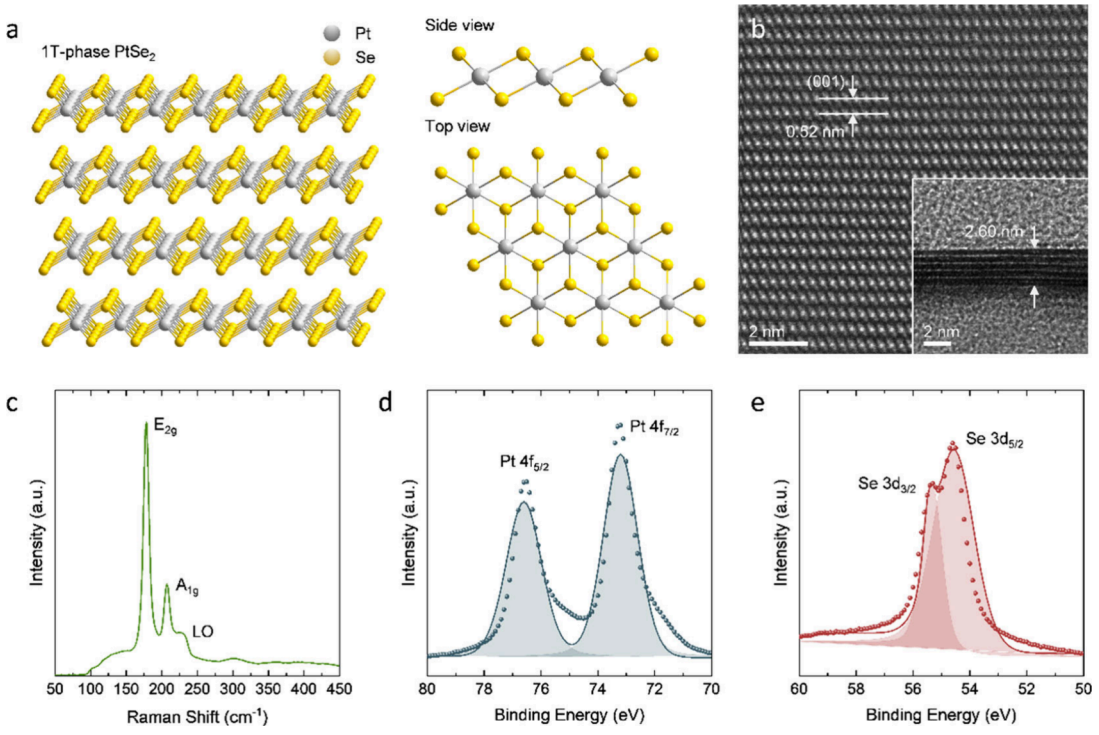

Figure 2. Structural and chemical characterization of CVD-grown $PtSe_2$ nanosheets. (a) Schematic of the 1T-phase $PtSe_2$ crystal structure with side and top views. (b) HR-STEM image of $PtSe_2$ nanosheets showing a periodic interlayer spacing of (001) planes. The inset displays a cross-sectional image measuring a thickness of 2.6 nm. (c) Raman spectrum of $PtSe_2$ nanosheets. (d, e) XPS profiles of the Pt 4f and Se 3d orbitals of $PtSe_2$ nanosheets.

while preserving material integrity. Recent studies have shown effective modulation of transport properties in 2D materials via SCTD. For instance, few-layer $PtSe_2$ exhibits strong ambipolar transport behavior due to its indirect band overlap, making it responsive to chemical doping. Youn et al. used benzyl viologen (BV) as an electron donor and magic blue (MB) as an electron acceptor to achieve n-type and p-type doping, respectively, via drop-casting.[5] This approach successfully suppressed the ambipolar characteristics of $PtSe_2$, yielding an improved power factor. In optoelectronics, area-selective SCTD has been applied to create p−n junctions within a single nanosheet. Choi et al.[6] used $AuCl_3$ to selectively dope n-

https://doi.org/10.1021/acsenergylett.5c02461
ACS Energy Lett. 2025, 10, 6466−6473

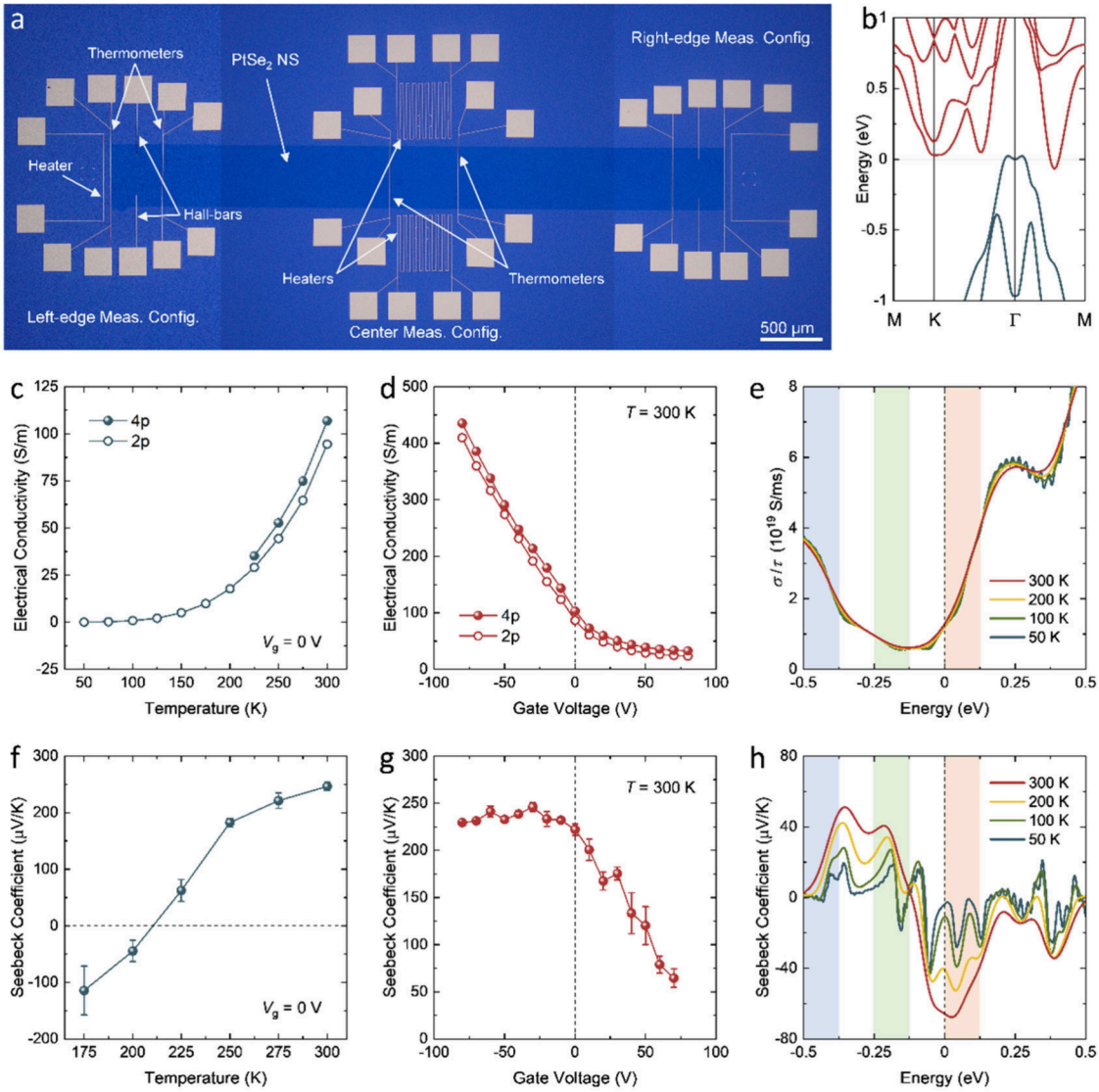

Figure 3. Transport properties of pristine five-layer $PtSe_2$ nanosheets. a) Optical image of microdevice fabricated via lithography and metallization. b) Band structure of trilayer $PtSe_2$ nanosheets calculated using first-principles density functional theory (DFT), showing indirect band overlap. (c,f) Temperature-dependent (c) electrical conductivity and (f) Seebeck coefficient at zero gate voltage. (d,g) Gate-tuned (d) electrical conductivity and (g) Seebeck coefficient at 300 K. (e,h) Theoretically predicted (e) electrical conductivity and (h) Seebeck coefficient obtained by solving the Boltzmann transport equation based on the DFT calculations for different temperatures (50, 100, 200, and 300 K). Theoretical data in (b), (e), and (h) are adapted with permission from ref 4. Copyright 2019 American Chemical Society.

type MoS_2 into p-type, and Sun et al.[7] converted p-type WSe_2 into n-type by applying hydrazine to form a lateral homojunction p−n diode. However, no study has demonstrated p−n junction formation via SCTD, specifically for thermoelectric applications. In this study, we propose a surface-doped p−n junction thermocouple based on a five-layer $PtSe_2$ nanosheet. Using BV and MB as electron donor and acceptor molecules, respectively, we selectively doped left and right regions through a nondestructive SCTD method. The resulting thermocouple exhibited high sensitivity to small temperature differences, demonstrating potential as a self-powered temperature sensor for integrated electronics and biomedical sensing. The SCTD technique provides a simple strategy for fabricating lateral p−n homojunctions based on 2D materials, offering utility across electronic devices.

Figure 1 shows the purpose and approach of this study. By fabricating a surface-doped $PtSe_2$ p−n homojunction and measuring its thermoelectric performance, we aimed to demonstrate the feasibility of this structure as a self-powered temperature sensor and to verify the effectiveness of SCTD (Figure 1a). We fabricated a simplified device with a $PtSe_2$ nanosheet and performed area-selective surface doping using a polydimethylsiloxane (PDMS) mask (Figure 1b). This process imparted p- and n-type characteristics to different regions of the $PtSe_2$ nanosheets (Figure 1c). Finally, thermoelectric measurements were conducted to evaluate whether the resulting p−n homojunction exhibited performance suitable for temperature sensing.

To fabricate surface-doped p−n junction thermocouples, dimension-defined $PtSe_2$ nanosheets were synthesized via chemical vapor deposition (CVD) and their structural and chemical characteristics were investigated as shown in Figure 2. 1T-phase $PtSe_2$ nanosheet exhibits a layered structure with van der Waals interaction where Pt atoms are sandwiched between

https://doi.org/10.1021/acsenergylett.5c02461
ACS Energy Lett. 2025, 10, 6466−6473

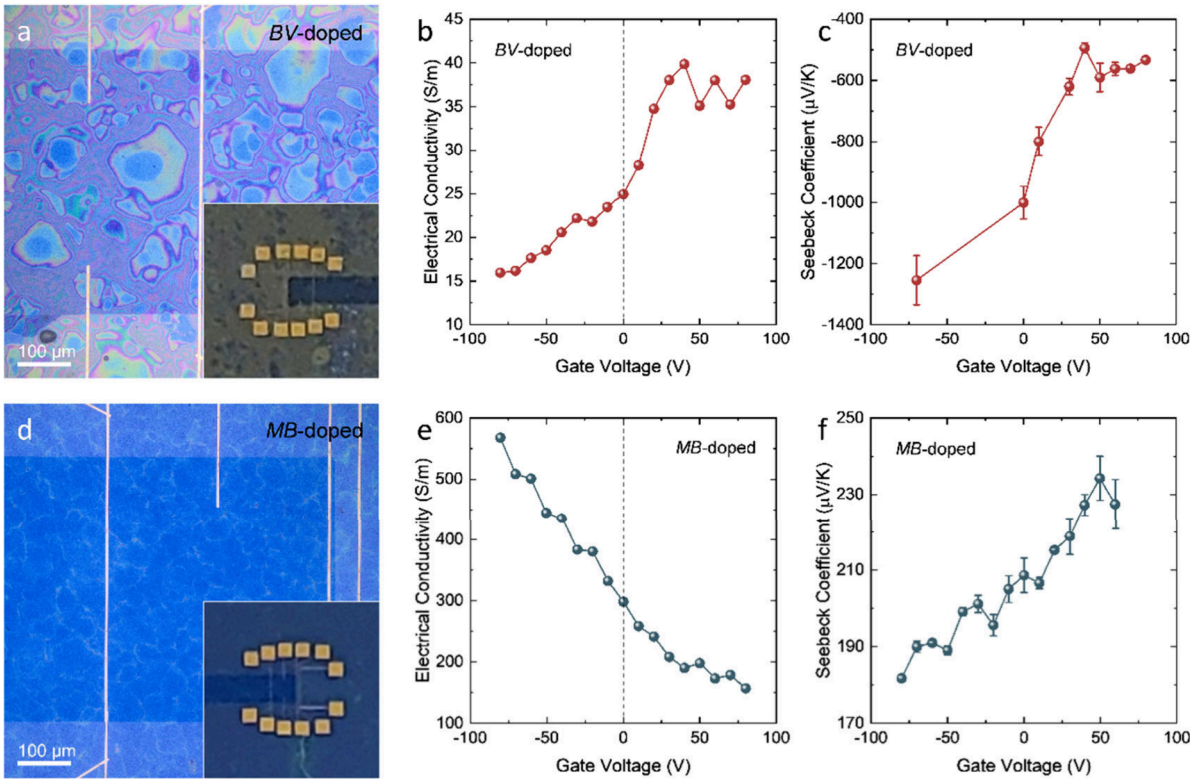

Figure 4. Transport properties of BV- and MB-doped five-layer $PtSe_2$ nanosheets. (a,d) Optical images of microdevices with (a) BV and (d) MB doping applied using the area-selective airbrush spray-coating. (b,e) Gate-dependent electrical conductivity at 300 K for (b) BV-doped and (e) MB-doped regions. (c,f) Gate-dependent Seebeck coefficient at 300 K for (c) BV-doped and (f) MB-doped regions.

upper and lower Se atoms (Figure 2a).[4,8] The 1T-phase atomic arrangement was confirmed by side-view high-resolution scanning transmission electron microscopy (HR-STEM) image of vertically sliced thick $PtSe_2$ sample, showing periodic interlayer spacing of 0.52 nm, matching previously reported results (Figure 2b).[9,10] For effective carrier-type-modulation through SCTD, five-layer $PtSe_2$ nanosheets exhibiting strong semimetallic characteristics were chosen as the pristine sample for p−n junction thermocouple fabrication (see inset of Figure 2b and Figure S1, Supporting Information).[5] The Raman spectra confirmed the phase of pristine $PtSe_2$, showing two peaks at 178.6 (E_{2g} in-plane mode) and 207.1 cm^{-1} (A_{1g} out-of-plane mode) (Figure 2c), consistent with previous results of single-crystalline 1T phase $PtSe_2$.[11] X-ray photoelectron spectroscopy (XPS) spectrum analysis of Pt 4f and Se 3d revealed deconvoluted peaks at ∼76.6 and 73.2 eV, corresponding to the $4f_{5/2}$ and $4f_{7/2}$ orbitals of Pt^{2+}, respectively (Figure 2d). In the Se 3d spectrum, the peaks at 55.3 and 54.6 eV are ascribed to the Se $3d_{3/2}$ and $3d_{5/2}$ orbitals, respectively (Figure 2e). These peaks match previously reported results and are used to confirm SCTD.[12,13]

To confirm the semimetallic behavior of the pristine five-layer $PtSe_2$, we investigated its transport properties and validated the results with theoretical calculations (Figure 3). The electrical conductivity and Seebeck coefficient of the nanosheets exhibited ambipolar transport characteristics predicted by the semimetallic band structure. Figure 3a shows the optical image of a microdevice fabricated via lithography and metallization to measure electrical conductivity and thermopower by creating temperature gradients under various conditions using heater and thermometer circuits (see Figure S2, Supporting Information). Figure 3b presents the band structure of trilayer $PtSe_2$ nanosheets obtained from first-principles density functional theory (DFT), as reported in our previous study.[4] Theoretical predictions suggest that nanosheets of this thickness exhibit semimetallic behavior with indirect band overlap. In addition, thinner nanosheets show bandgaps and semiconducting properties, whereas thicker ones display metallic characteristics.[4,10] We examined the temperature-dependent electrical conductivity of the pristine nanosheets using thermometer electrodes, measuring resistance from the voltage signal in the range of 50−300 K. The results show increased electrical conductivity with rising temperature (Figure 3c). This behavior stems from reduced band overlap in confined dimensions, leading to semimetallic, rather than metallic, transport characteristics, which are observed in bulk crystals.[4,14] Four-probe measurements were performed to determine and exclude contact resistance, and the results were consistent with two-probe results without significant deviations that could impact the experimental outcomes. Gate-dependent conductivity measured within − 80 to 80 V (Figure 3d) revealed strong gate dependence with positive values and negative slopes, indicating holes as majority carriers while demonstrating the existence of ambipolar transport characteristics. This observation aligns with predictions based on the semimetallic band structure and matches the green-highlighted region in theoretical results from Boltzmann transport equation calculations (Figure 3e). The Seebeck coefficient calculations (see Figure S2, Supporting Information) support the ambipolar transport characteristics of the five-layer $PtSe_2$ nanosheet. Figure 3f shows that the Seebeck coefficient increases from negative to positive with rising temperature, indicating that thermal excitation of holes changes the dominant carrier type from electrons to holes. As shown in

https://doi.org/10.1021/acsenergylett.5c02461
ACS Energy Lett. 2025, 10, 6466−6473

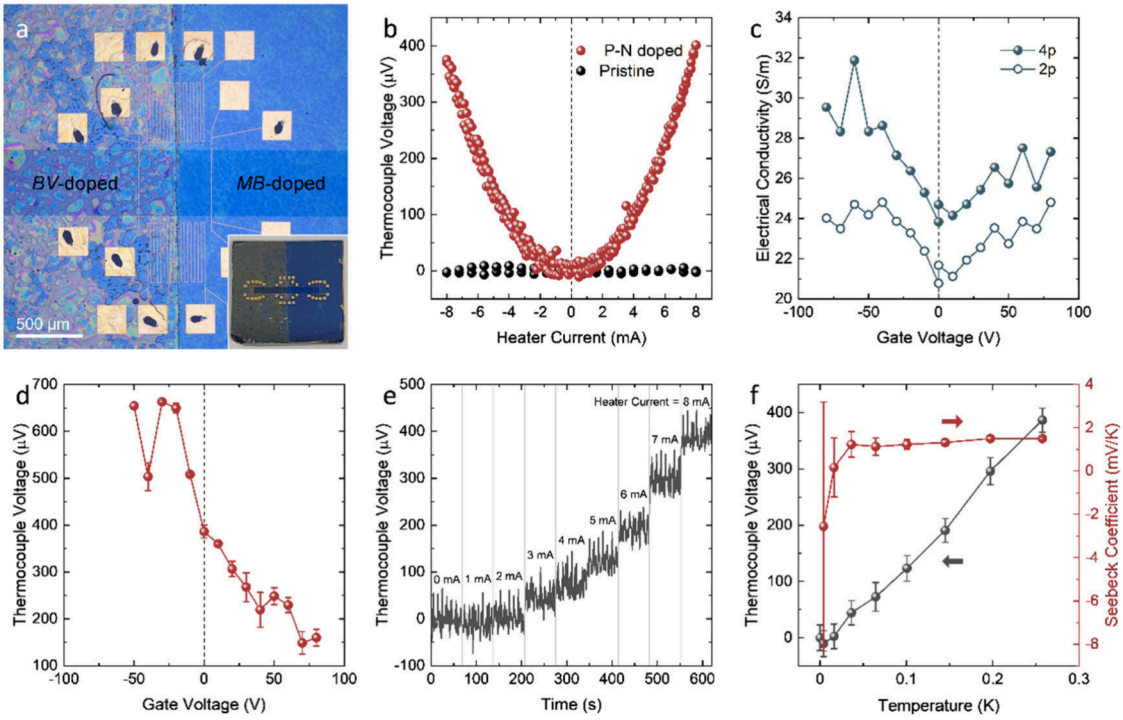

Figure 5. Thermoelectric properties and temperature sensing performance of the $PtSe_2$ p−n homojunction thermocouple. (a) Optical image of the device fabricated via SCTD. (b) Thermocouple voltage as a function of heater current before (black) and after (red) area-selective p−n doping. (c) Gate-dependent electrical conductivity of the surface-doped $PtSe_2$ nanosheet. (d) Gate-dependent thermocouple voltage measured between electrodes on the BV- and MB-doped regions of the nanosheet. (e) Real-time thermocouple voltage response under varying heater currents. (f) Thermocouple voltage and Seebeck coefficient as functions of the temperature difference.

Figure 3g, the decrease in Seebeck coefficient with increasing gate voltage results from reduced hole concentration and electrical conductivity at positive gate voltages. These semimetallic behaviors are supported by theoretical predictions illustrated in Figure 3h. In conclusion, the experimental results demonstrate that the five-layer $PtSe_2$ nanosheets exhibit sufficient ambipolar transport characteristics to enable effective modulation of transport properties via SCTD.

To induce and verify n-type and p-type characteristics independently on each side of the five-layer $PtSe_2$ nanosheet, BV and MB layers were deposited to opposite halves of the microdevice by area-selective airbrush spray-coating (see Figure S3, Supporting Information). Transport properties were measured to assess doping effects (Figure 4). BV was applied on the left side to introduce n-type doping (Figure 4a and inset). The gate-dependent electrical conductivity of the BV-doped region at 300 K showed a positive slope, indicating that electrons became majority carriers (Figure 4b). This contrasts with the pristine sample in Figure 3d, confirming n-type characteristics were induced. The n-type behavior is further supported by the negative Seebeck coefficient (Figure 4c). The positive slope with respect to the gate voltage reflects the suppression of minority carrier effect, consistent with the red area in the theoretical prediction results shown in Figure 3h. These results indicate that BV molecules successfully donate electrons to the nanosheet. MB was deposited as a p-type dopant on the right side of the nanosheets (Figure 4d and inset). The electrical conductivity of the MB-doped region decreased with increasing gate voltage, showing holes remained majority carriers, as in the pristine sample (Figure 4e). Enhanced electrical conductivity suggests reinforced p-type transport characteristics via MB molecules. This is further supported by the positive Seebeck coefficient, which (unlike the results shown in Figure 3g), increased with higher gate voltage (Figure 4f). This result indicates that MB doping suppresses the ambipolar transport characteristics of the pristine nanosheets, thereby enhancing the hole-dominated thermoelectric properties (blue area in Figure 3h).[5] In conclusion, our experimental results demonstrate that transport properties of semimetallic five-layer $PtSe_2$ nanosheets can be controlled using SCTD with BV and MB, aligning with previous reports on semimetallic $PtSe_2$ nanosheets doped by drop-casting.[5,10] The induced n-type and p-type transport characteristics are further described by temperature dependence and Hall measurement results in Figures S4 and S5 (Supporting Information).

Figure 5 shows the thermoelectric properties and sensing performance of the $PtSe_2$ p−n homojunction thermocouple fabricated via area-selective SCTD. As shown in Figure 5a, the device comprises a $PtSe_2$ nanosheet where left and right regions were selectively doped with BV and MB. Heaters in the center applied a lateral temperature gradient for thermoelectric measurement. As shown in Figure 5b, while no thermocouple signal was observed before doping, a clear thermoelectric voltage response appeared due to Seebeck coefficient differences between regions after selective doping (see Figure S6a, Supporting Information). This signal increased with heater current, demonstrating successful p−n junction thermocouple formation. The gate-dependent electrical conductivity showed bipolar behavior due to doping effects from n-type and p-type regions (Figure 5c). Figure 5d presents the gate-dependent thermocouple voltage between the two ends of the nanosheets. Such gate modulation of the thermoelectric output indicates that the sensing performance can be tuned by electrostatic

https://doi.org/10.1021/acsenergylett.5c02461
ACS Energy Lett. 2025, 10, 6466−6473

control of the charge-transport state, suggesting the potential for gate-adjustable temperature sensitivity. The temperature difference between the center (p−n junction) and the electrodes at an 8-mA heater current was measured using thermometers at the center and end of the nanosheet. The potential overestimation of the Seebeck coefficient, which may arise from the temperature difference between the junction and the center heater position, was evaluated using the Seebeck coefficients obtained from Figure 4c and 4f (see Figure S6b and S6c, Supporting Information). In Figure 5e, the real-time thermocouple voltage response increases with the heater current, revealing clear stepwise changes correlated with the temperature gradient. Figure 5f presents the thermocouple voltage as a function of the temperature difference. The resulting coefficient remains nearly constant over the range of heater currents, indicating stable thermoelectric response under varying thermal inputs. This stability was also well maintained under vacuum conditions (Figure S7, Supporting Information). Considering the measurement uncertainty and noise, the minimum estimated detectable temperature difference was below 0.1 K, indicating a sensing resolution in the sub-0.1 K range. In addition, passive operation allowed real-time temperature readout without external power.

In this study, we demonstrated effective tuning of the transport properties of semimetallic $PtSe_2$ nanosheets via SCTD, and successfully fabricated a lateral p−n homojunction thermocouple. While the pristine nanosheets exhibited ambipolar transport behavior, our area-selective airbrush method, leveraging BV and MB molecular dopants, enabled independent formation of n-type and p-type regions on a single five-layer $PtSe_2$ nanosheet. The fabricated thermocouple enabled real-time temperature sensing without external power and exhibited a high resolution, thus detecting temperature differences below 0.1 K. These results show that SCTD is an effective, damage-free method for precise control of charge carrier type in various 2D materials, offering a scalable strategy for thermoelectric systems and broader electronic applications.

EXPERIMENTAL METHODS

Synthesis. Dimension-defined 2D $PtSe_2$ nanosheets was synthesized using a homemade four-inch lateral quartz tube furnace. The channel region was patterned via photolithography using a mask aligner (Midas MDA-600S), followed by the deposition of Pt layers onto the growth substrates (1.6 cm × 1.6 cm SiO_2/Si) by electron beam evaporation at a rate of 0.1 Å/s. Dimethyl selenide ($(CH_3)_2Se$) was chosen as the Se precursor, which vaporized at room temperature. The precursor decomposed at 650 °C in the heating zone and subsequently reacted with the predeposited Pt in the growth zone at 450 °C. The growth substrate was carefully placed at the center of the reaction zone to ensure uniformity. The gas flow rates were precisely controlled using mass flow controllers. Ar gas served as the carrier gas to transport the decomposed Se precursor, while O_2 was introduced to eliminate residual carbon contaminants from $(CH_3)_2Se$. For optimal synthesis conditions, the flow rates were set to 500, 20, and 5 sccm for Ar, O_2, and $(CH_3)_2Se$, respectively, and the chamber pressure was maintained at approximately 80 Torr throughout the growth process.

Device Fabrication. The structural properties of the $PtSe_2$ nanosheets were analyzed using various characterization techniques, including TEM (JEM-ARM 200F, Jeol), dual-beam focused ion beam (Crossbeam 540, ZEISS), Raman spectroscopy with a 532 nm laser (LabRam ARAMIS, Horiba Scientific), XPS (K-alpha, Thermo Fisher Scientific, Inc.), and atomic force microscopy (XE-150, Park Systems).[5,15,16] The microdevices used in transport measurements were fabricated using electron-beam lithography (VEGA3, Tescan and NPGS, JC Nabity Lithography Systems) and a subsequent lift-off process. To improve the electrical contact between the $PtSe_2$ nanosheet and electrodes, the patterned nanosheet was subjected to Ar plasma treatment for 20 s prior to Cr (5 nm)/Au (100 nm) metallization, which was performed using a custom-designed plasma etching and sputtering system.[4,15−20]

Surface Charge-Transfer Doping Using the Synthesized BV and MB Dopants. For the n-type SCTD, BV dopants were synthesized using 1,1′-dibenzyl-4,4′-bipyridinium dichloride (Sigma−Aldrich, 97%). Specifically, 16.35 mg of BV dichloride was dissolved in 4 mL of deionized water, followed by the addition of 4 mL of toluene to form a toluene−water bilayer. To facilitate the reduction of BV^{2+} ions in BV dichloride to BV^0, 40 mg of $NaBH_4$ (Sigma−Aldrich) was introduced into the solution. After 24 h of stirring, the upper toluene layer containing the resulting BV solution (10 mM) was extracted using a micropipette. Further details on this procedure are reported elsewhere.[21,22] For the p-type SCTD, MB solutions (0.5 mM) were prepared by dissolving 20.41 mg of tris(4-bromophenyl) ammoniumyl hexachloroantimonate (Sigma−Aldrich) in 5 mL of anhydrous dichloromethane.[23] For molecular doping, the BV dopant was airbrushed onto the left half of the patterned $PtSe_2$ microdevice, whereas the MB dopant was airbrushed onto the right half; both the steps were performed at 50 °C for approximately 15 min each using a 0.4 mm-thick PDMS mask (Figure S3, Supporting Information).

Transport Property Measurements. The microdevice included electrodes functioning as heaters and near and far thermometers, positioned at the center and both ends of the $PtSe_2$ nanosheet. The electrical conductivity of the device was evaluated, under high vacuum conditions, using $V-I$ and $I-V$ measurement systems (2182 nanovoltmeter and 236 source meter, Keithley). To determine the Seebeck coefficient, the voltage difference between the near-TM and far-TM thermometers was measured with a nanovoltmeter. The temperature difference was derived from the temperature coefficient of resistance of each thermometer, assessed using a lock-in amplifier (SR850, Stanford Research Systems). All the measurements were performed in a closed-cycle cryostat (X-1AL, Advanced Research Systems) under high vacuum conditions ($<5 \times 10^{-6}$ Torr) to minimize thermal fluctuations.

Theoretical Calculations. First-principles DFT calculations were carried out using the projector augmented wave method as implemented in the Vienna Ab initio Simulation Program code.[24] The generalized gradient approximation with the Perdew−Burke−Ernzerhof exchange-correlation functional was employed, including spin−orbit coupling.[25,26] The slab supercell model of trilayer structure was constructed with a vacuum spacing of 15 Å along the c-axis to prevent spurious interactions. van der Waals interactions were accounted for using the DFT-D3 method with Becke−Johnson damping.[27,28] A 56 × 56 × 1 k-point mesh was used, and the plane-wave energy cutoff was set to 700 eV. The structural optimization was performed until the Hellmann−Feynman forces on each atom were less than 10^{-5} eV $Å^{-1}$.

https://doi.org/10.1021/acsenergylett.5c02461
ACS Energy Lett. 2025, 10, 6466−6473

■ ASSOCIATED CONTENT

Supporting Information

The Supporting Information is available free of charge at https://pubs.acs.org/doi/10.1021/acsenergylett.5c02461.

Experimental details, additional optical, electrical, and AFM characterization data, numerical simulation, and additional discussion (PDF)

■ AUTHOR INFORMATION

Corresponding Authors

Jeongmin Kim − *Division of Nanotechnology, DGIST, Daegu 42988, Republic of Korea*; Email: jkim@dgist.ac.kr

Kibum Kang − *Department of Material Science and Engineering, Korea Advanced Institute of Science and Technology (KAIST), Daejeon 34141, Republic of Korea; Graduate School of Semiconductor Technology, Korea Advanced Institute of Science and Technology (KAIST), Daejeon 34141, Republic of Korea;* orcid.org/0000-0003-1674-1826; Email: kibumkang@kaist.ac.kr

Wooyoung Lee − *Department of Materials Science and Engineering, Yonsei University, Seoul 03722, Republic of Korea;* orcid.org/0000-0001-8406-4324; Email: wooyoung@yonsei.ac.kr

Authors

Seonhye Youn − *Department of Materials Science and Engineering, Yonsei University, Seoul 03722, Republic of Korea*

Sangkil Lee − *Department of Materials Science and Engineering, Yonsei University, Seoul 03722, Republic of Korea*

Minseung Gyeon − *Department of Material Science and Engineering, Korea Advanced Institute of Science and Technology (KAIST), Daejeon 34141, Republic of Korea;* orcid.org/0009-0007-5101-6351

Joonho Bang − *School of Materials Science and Engineering, Gyeongsang National University, Jinju 52828, Republic of Korea; Department of Materials Engineering and Convergence Technology, Gyeongsang National University, Jinju 52828, South Korea*

Taehoo Chang − *Department of Materials Science and Engineering, Incheon National University, Incheon 22012, Republic of Korea;* orcid.org/0000-0002-3905-8301

Hongjae Moon − *Department of Materials Science and Engineering, Yonsei University, Seoul 03722, Republic of Korea*

Dong Hwan Kim − *Division of Nanotechnology, DGIST, Daegu 42988, Republic of Korea*

Complete contact information is available at: https://pubs.acs.org/10.1021/acsenergylett.5c02461

Author Contributions

S.Y., J.K., S.L., and M.G. contributed equally to this work.

Notes

The authors declare no competing financial interest.

■ ACKNOWLEDGMENTS

This work was supported by the the Deep Science Startup Promotion Program (RS-2025-02633929) supported by Commercializations Promotion Agency for R&D Outcomes (COMPA), the National Research Foundation of Korea (NRF) grant funded by the Korea government (MSIT) (No. NRF-2022M3H4A3053304, National Core Materials Research Center (Platform type)), and Technology Innovation Program ("2410004860", Center for Super Critical Material Industrial Technology) funded By the Ministry of Trade, Industry & Energy(MOTIE, Korea) . J.K. acknowledges support from the National Research Foundation of Korea (RS-2023-00211034 and RS-2021-NR060108) and the DGIST R&D Program (25-ET-02). K.K. acknowledges support from the National Research Foundation of Korea (NRF) grants funded by the Korea government (MSIT) (RS-2023-00258309). The authors also thank Jung Woo Ha (DGIST) for illustration assistance.

■ REFERENCES

(1) Huang; Luo, X.; Gan, C. K.; Quek, S. Y.; Liang, G. Theoretical Study of Thermoelectric Properties of Few-Layer MoS_2 and WSe_2. *Phys. Chem. Chem. Phys.* **2014**, *16* (22), 10866−74.

(2) Yoshida; Iizuka, T.; Saito, Y.; Onga, M.; Suzuki, R.; Zhang, Y.; Iwasa, Y.; Shimizu, S. Gate-Optimized Thermoelectric Power Factor in Ultrathin WSe_2 Single Crystals. *Nano Lett.* **2016**, *16* (3), 2061−65.

(3) Pang; Bachmatiuk, A.; Yin, Y.; Trzebicka, B.; Zhao, L.; Fu, L.; Mendes, R. G.; et al. Applications of Phosphorene and Black Phosphorus in Energy Conversion and Storage Devices. *Adv. Energy Mater.* **2018**, *8* (8), No. 1702093.

(4) Moon; Bang, J.; Hong, S.; Kim, G.; Roh, J. W.; Kim, J.; Lee, W. Strong Thermopower Enhancement and Tunable Power Factor via Semimetal to Semiconductor Transition in a Transition-Metal Dichalcogenide. *ACS Nano* **2019**, *13* (11), 13317−24.

(5) Youn; Kim, J.; Moon, H.; Kim, J.-K.; Jang, J.; Chang, J.; Lee, T.; Kang, K.; Lee, W. Enhanced Thermoelectric Power Factor in Carrier-Type-Controlled Platinum Diselenide Nanosheets by Molecular Charge-Transfer Doping. *Small* **2022**, *18* (23), No. 2200818.

(6) Choi; Qu, D.; Lee, D.; Liu, X.; Watanabe, K.; Taniguchi, T.; Yoo, W. J. Lateral MoS_2 P−N Junction Formed by Chemical Doping for Use in High-Performance Optoelectronics. *ACS Nano* **2014**, *8* (9), 9332−40.

(7) Sun; Xie, D.; Sun, Y.; Li, W.; Ren, T. Locally Hydrazine Doped WSe_2 PN Junction toward High-Performance Photodetectors. *Nanotechnology* **2018**, *29* (1), No. 015203.

(8) Kliche. Far-Infrared and X-Ray Investigations of the Mixed Platinum Dichalcogenides $PtS_{2-x}Se_x$, $PtSe_{2-x}Te_x$, and $PtS_{2-x}Te_x$. *J. Solid State Chem.* **1985**, *56* (1), 26−31.

(9) Zhang; Yan, M.; Zhang, H.; Huang, H.; Arita, M.; Sun, Z.; Duan, W.; Wu, Y.; Zhou, S. Experimental Evidence for Type-II Dirac Semimetal in $PtSe_2$. *Phys. Rev. B* **2017**, *96* (12), No. 125102.

(10) Kim; Youn, S.; Bang, J.; Moon, H.; Jang, W.; Roh, J. W.; Kim, D. H.; Chang, J.; Lee, W. Experimental Verification of Semimetallic Band Structure in $PtSe_2$ via Thermoelectric Power Measurements. *Appl. Phys. Lett.* **2022**, *120* (4), 043103.

(11) O'Brien; McEvoy, N.; Motta, C.; Zheng, J.-Y.; Berner, N. C.; Kotakoski, J.; Elibol, K.; et al. Raman Characterization of Platinum Diselenide Thin Films. *2D Materials* **2016**, *3* (2), No. 021004.

(12) Jiang; Wang, X.; Chen, Y.; Wu, G.; Ba, K.; Xuan, N.; Sun, Y.; et al. Large-Area High Quality $PtSe_2$ Thin Film with Versatile Polarity. *InfoMat* **2019**, *1* (2), 260−67.

(13) Xie; Zhang, D.; Yan, X.-Q.; Ren, M.; Zhao, X.; Liu, F.; Sun, R.; et al. Optical Properties of Chemical Vapor Deposition-Grown $PtSe_2$ Characterized by Spectroscopic Ellipsometry. *2D Materials* **2019**, *6* (3), No. 035011.

(14) Ciarrocchi; Avsar, A.; Ovchinnikov, D.; Kis, A. Thickness-Modulated Metal-to-Semiconductor Transformation in a Transition Metal Dichalcogenide. *Nat. Commun.* **2018**, *9* (1), 919.

(15) Moon; Kim, J.; Bang, J.; Hong, S.; Youn, S.; Shin, H.; Roh, J. W.; Shim, W.; Lee, W. Semimetallic Features in Thermoelectric Transport Properties of 2H−3R Phase Niobium Diselenide. *Nano Energy* **2020**, *78*, No. 105197.

(16) Youn; Kim, J.; Lee, H.; Kim, D. H.; Bang, J.; Lee, W. Strong Anisotropic Transport Properties of Quasi-One-Dimensional $ZrTe_3$ Nanoribbons. *Nano Energy* **2024**, *127*, No. 109771.

(17) Kim; Lee, S.; Brovman, Y. M.; Kim, P.; Lee, W. Diameter-Dependent Thermoelectric Figure of Merit in Single-Crystalline Bi Nanowires. *Nanoscale* **2015**, *7* (11), 5053−59.
(18) Yoo; Kim, J.; Moon, H.; Kim, S. Y.; Ko, D.; Shin, W. H.; Hwang, S.; et al. Strong Enhancement of Electrical Conductivity in Two-Dimensional Micrometer-Sized RuO_2 Nanosheets for Flexible Transparent Electrodes. *Nanoscale* **2017**, *9* (21), 7104−13.
(19) Kim; Youn, S.; Go, T. W.; Kim, J.; Yoo, C.; Shawkat, M. S.; Han, S. S.; et al. Revealing Pt-Seed-Induced Structural Effects to Tribological/Electrical/Thermoelectric Modulations in Two-Dimensional $PtSe_2$ Using Scanning Probe Microscopy. *Nano Energy* **2022**, *91*, No. 106693.
(20) Kim; Youn, S.; Lee, D.; Kim, C. W.; Moon, H.; Chung, S.-H.; Kim, H.; et al. Electrical Transport Phenomena in Two-Dimensional Metallic 2H-$NbSe_2$: An Experimental and Theoretical Study. *Nanoscale* **2024**, *16* (48), 22230−39.
(21) Kim; Jang, J. H.; Kim, K. K.; Park, H. K.; Bae, J. J.; Yu, W. J.; Lee, I. H.; et al. Reduction-Controlled Viologen in Bisolvent as an Environmentally Stable N-Type Dopant for Carbon Nanotubes. *J. Am. Chem. Soc.* **2009**, *131* (1), 327−31.
(22) Kiriya; Tosun, M.; Zhao, P.; Kang, J. S.; Javey, A. Air-Stable Surface Charge Transfer Doping of MoS_2 by Benzyl Viologen. *J. Am. Chem. Soc.* **2014**, *136* (22), 7853−56.
(23) Zhang, S.; Hill, H. M.; Moudgil, K.; Richter, C. A.; Hight Walker, A. R.; Barlow, S.; Marder, S. R.; Hacker, C. A.; Pookpanratana, S. J. Controllable, Wide-Ranging N-Doping and P-Doping of Monolayer Group 6 Transition-Metal Disulfides and Diselenides. *Adv. Mater.* **2018**, *30* (36), No. 1802991.
(24) Kresse; Furthmüller, J. Efficient Iterative Schemes for *Ab initio* Total-Energy Calculations Using a Plane-Wave Basis Set. *Phys. Rev. B* **1996**, *54* (16), 11169.
(25) Steiner; Khmelevskyi, S.; Marsmann, M.; Kresse, G. Calculation of the Magnetic Anisotropy with Projected-Augmented-Wave Methodology and the Case Study of Disordered $Fe_{1-x}Co_x$ Alloys. *Phys. Rev. B* **2016**, *93* (22), No. 224425.
(26) Perdew; Burke, K.; Ernzerhof, M. Generalized Gradient Approximation Made Simple. *Phys. Rev. Lett.* **1996**, *77* (18), 3865.
(27) Grimme, S.; Ehrlich; Goerigk, L. Effect of the Damping Function in Dispersion Corrected Density Functional Theory. *J. Comput. Chem.* **2011**, *32* (7), 1456−65.
(28) Grimme; Antony, J.; Ehrlich, S.; Krieg, H. A Consistent and Accurate *Ab initio* Parametrization of Density Functional Dispersion Correction (DFT-D) for the 94 Elements H-Pu. *The Journal of Chemical Physics* **2010**, *132* (15), 154104.

https://doi.org/10.1021/acsenergylett.5c02461
ACS Energy Lett. 2025, 10, 6466−6473